Can. J. Remote Sensing, Vol. 30, No. 4, pp. 593–603, 2004

Application of remotely sensed data to the assessment of terrain factors affecting the Tsao-Ling landslide

M.D. Yang, Y.F. Yang, and S.C. Hsu

Abstract. The Chi-Chi earthquake, the most severe natural disaster of the last century in Taiwan, struck the west-central part of the island in the very early morning on 21 September 1999. This serious earthquake changed the landscape of central Taiwan. The strong natural motion triggered thousands of landslides and debris flows in the hills and mountains. Tsao-Ling Lake was formed by massive landslides that blocked Chinshui Creek. Besides geological conditions, terrain factors such as slope, aspect, and vegetation greatly affect the stability of the slopes. To monitor and evaluate the locations and variations of the landslide scars in the Chinshui watershed, remote sensing techniques were applied to provide temporal and spatial information. Airborne and satellite imagery was adopted to help in the collection of terrain information. Aerial photographs and SPOT satellite images were processed to assess the damage level of slide areas and the potential risk of landslide reoccurrence in the watershed of the Tsao-Ling area. The overall affecting scores combining three terrain factors were processed by an aggregation function to produce a synthetic probability map of landslide reoccurrence. The probability of landslide reoccurrence in the Tsao-Ling area can be a reference for decision-makers to efficiently locate areas with high probability of landslide occurrence and create treatment and rehabilitation plans.

Résumé. Le séisme de Chi-Chi, le désastre naturel le plus dévastateur du dernier siècle à Taiwan, a frappé la partie centrale ouest de l'île très tôt le matin du 21 septembre 1999. Le séisme de forte amplitude a transformé le paysage du centre de Taiwan. L'érosion naturelle intense dans la région a généré des milliers de marques d'érosion sur les collines et les montagnes. Le lac Tsao-Ling a été formé par des glissements de terrain massifs bloquant le Chinshui Creek. En plus des conditions géologiques, des facteurs de terrain tels que le degré de pente, l'orientation et la végétation affectent considérablement la stabilité des pentes. Pour réaliser le suivi et évaluer les sites et les variations de ces marques dans le bassin versant, les techniques de télédétection ont été appliquées afin d'apporter une information temporelle et spatiale. Nous avons utilisé des images aéroportées et satellitaires pour aider à la collecte d'information sur le terrain. Les photographies aériennes et les images satellitaires SPOT ont été traitées pour évaluer le niveau de dommage au niveau des zones défoncées et le risque potentiel pour le bassin versant de la zone de Tsao-Ling. Les scores globaux combinant trois facteurs de terrain ont été traités à l'aide d'une fonction d'agrégation pour produire une carte synthétique de probabilité de ré-occurrence de glissement de terrain. La probabilité de ré-occurrence de glissement de terrain dans la région de Tsao-Ling peut constituer une référence pour les décideurs afin qu'ils puissent localiser plus efficacement les zones présentant une probabilité élevée d'occurrence de glissement de terrain et mettre au point des plans de traitement et de redressement.
[Traduit par la Rédaction]

Introduction

The Chi-Chi earthquake (also known as the "921 earthquake", named after its date of occurrence) in Taiwan induced severe changes to the landscape. Several major slides blocked river valleys, resulting in landslide dams in central Taiwan. The dams are constructed from rock and fine-grained materials from the landslides. Owing to its unconsolidated and disturbed nature, this kind of natural dam is far from stable. The Tsao-Ling landslide is the largest landslide resulting from the 921 earthquake. A long-term observation program has been developed to monitor environmental variations in the Tsao-Ling region. The program includes soil investigation and monitoring of vegetation distribution, groundwater level, and the condition of spillways and hillsides. High resolution in topographic information is essential for disaster remediation and damage rehabilitation after an earthquake. This paper employs remote sensing techniques, including satellite imagery and airborne photogrammetry, and field survey to provide an economic and quick monitoring of the landslide area.

Terrain investigations resulting from natural disasters traditionally used ground surveys. These types of investigations require strenuous effort and considerable time and are more difficult in challenging environments after a natural disaster, such as heavy rain or earthquake. Because of this difficulty, engineers in Taiwan often cannot visit the disaster area to complete their surveying work. Data acquisition of the terrain

Received 8 July 2003. Accepted 27 February 2004.

M.D. Yang[1] and Y.F. Yang. Department of Civil Engineering, National Chung Hsing University, Taichung, Taiwan, Republic of China.

S.C. Hsu. Department of Construction Engineering, Chaoyang University of Technology, Taichung County, Taiwan, Republic of China.

[1]Corresponding author (e-mail: mdyang@dragon.nchu.edu.tw).

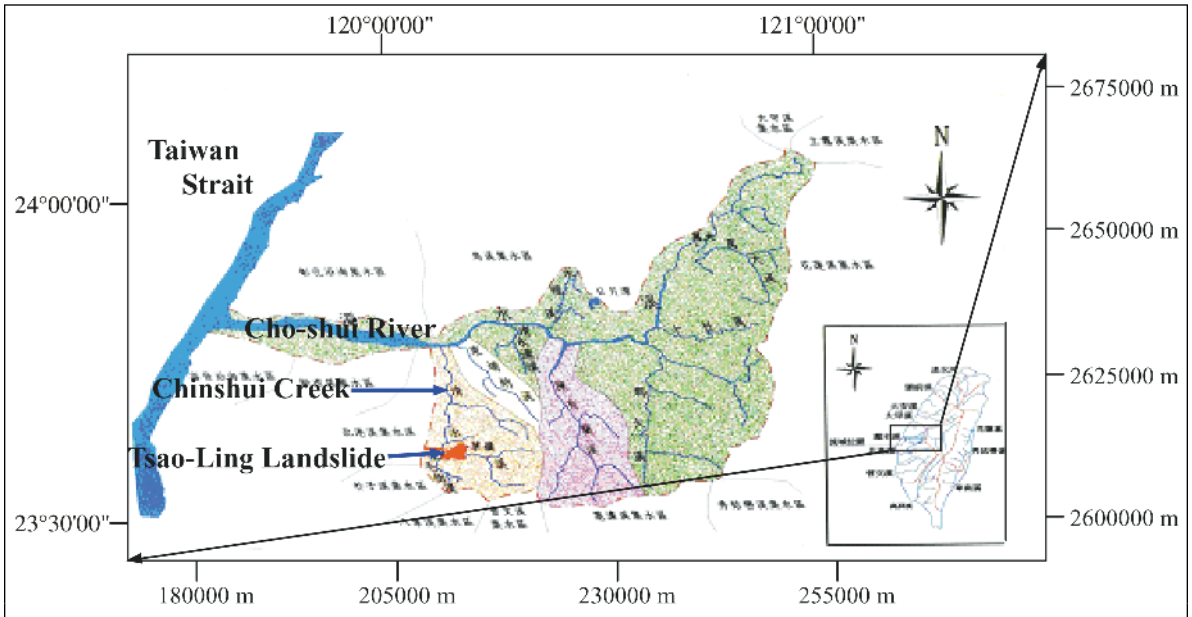

Figure 1. Location of the Tsao-Ling landslide region.

transition is needed as soon as possible to determine a timely and proper response to a natural disaster. A large-scale, efficient, quick investigation could be approached with an aerial survey and satellite imagery. In this paper, several affecting factors of the Tsao-Ling landslide are briefly described, and then a quantitatively analytical evaluation model is established and executed. Lastly, synthetic probability maps of landslide reoccurrence are produced that provide efficient information for planning an emergency response and a rehabilitation strategy.

Study site

The Tsao-Ling landslide is located near Chinshui Creek in the upper reach of the Cho-Shui River (see **Figure 1**) (Institute of Planning and Hydraulic Research, 1996). Rock and fine-grained materials from the Chinshui watershed filled a 5 km length of the river valley (over 1000 m wide and 50 m deep) as a natural dam. The Tsao-Ling landslide lake has a watershed area of approximately 160 km^2 at an elevation of 503 m above sea level. **Figures 2 and 3** are satellite images from SPOT before and after the 921 earthquake. The images were acquired on 28 January 1999 and 11 February 2000.

The Fourth Bureau of River Management, Water Conservancy Agency, Ministry of Economic Affairs, collected historical information to analyze the geological structure, water permeation, and surface runoff for the Tsao-Ling area after the 921 earthquake. According to the available literature, there were at least five catastrophic landslides that occurred in the Tsao-Ling area before the 921 earthquake. The main landslide events are listed in **Table 1** (Chang, 1984; Hsu and Leung, 1977; Hung, 1980; 2000). Based on a field examination and investigation, it was concluded that the major causes of the Tsao-Ling landslides were terrain characteristics, rock formation, geological structure, rainfall, and earthquake force (Water Conservancy Agency, 1999). The landslides were triggering mainly by earthquakes or heavy rainfall.

Geological conditions

The Tsao-Ling area is located 30 km northeast of Chiayi County in the Western Foothill Region of central Taiwan. The geological formations in the Tsao-Ling area are, from old to young, Shihliufen Shale, Dawuo Sandstone, Chinshui Shale, Cholan Formation, terrace deposits, alluvium, and colluvium. The major types of materials, thickness, and time of deposition for each formation are summarized in **Table 2**.

The formations in the landslide area consist of the Cholan Formation and underlying Chinshui Shale. The upper part of the Cholan Formation is mainly alternations of interbedded sandstone and shale overlying massive, dark gray Chinshui Shale. This bedrock forms a monocline with an anticline axis passing through the upstream side and a syncline axis through the downstream side (Chang, 1984). The dip direction of the formations inclines toward the valley and is about 235° from the north, i.e., southwestern direction. The measured dip angle ranges from 12° to 14°. These rocks have been jointed and fractured by tectonic movements, and the joints in the sandstone are usually clear openings that allow much more surface water to infiltrate and weaken the underlying shale. Joints resulting from pressure relief were also observed in the sandstones of previously formed cliffs. Few joints were found in the shale and mudstone. Since the sandstone formation is more permeable, the surface water usually seeps through the sandstone layer and stops at the shale or mudstone layers. Water seeps out from the interfaces of these different rock formations. Therefore, springs were frequently reported on both wings of the Tsao-Ling anticline near the collapsed area.

Figure 2. Tsao-Ling SPOT4 satellite image acquired on 28 January 1999. The rectangle is centred over the area of the major Tsao-Ling landslide.

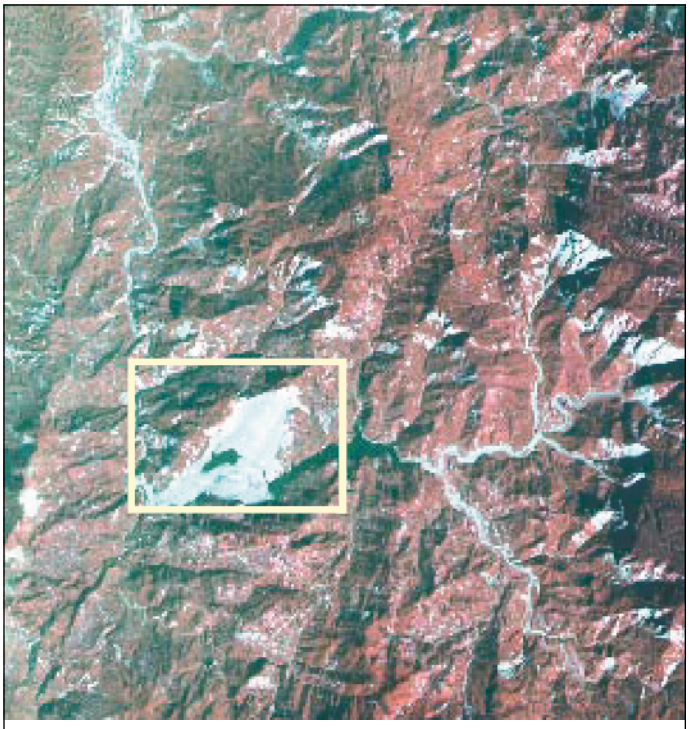

Figure 3. Tsao-Ling SPOT4 satellite image acquired on 11 February 2000. The major Tsao-Ling landslide is visible within the rectangle.

Table 1. Main landslide events in the Tsao-Ling area.

Date	Cause of slide[a]	Description	Failure of dam	Approx. height of dam (m)
June 1862	Earthquake (M = 6–7)	Landslide; formation of a natural dam	Failed in 1875	—
1888	Earthquake	Landslide; formation of a natural dam	Failed in 1898 because of heavy rainfall	—
17 Dec. 1941	Earthquake (M = 7.1)	Landslide; formation of a natural dam and a natural lake	—	140
10 Aug. 1942	Heavy rainfall	Landslide; formation of a natural dam; 137 deaths and 1200 houses destroyed	Overtopped in 1951	214[b]
14 Aug. 1979	Heavy rainfall	Landslide; 5 million cubic metres in volume; formation of a natural dam containing 40 million cubic metres of water	Overtopped in 1979; two bridges destroyed by the flooding	90
21 Sept. 1999	Earthquake (M = 7.3)	Landslide; 120 million cubic metres in volume; formation of a natural earth dam containing 26 million cubic metres of water; 36 deaths	—	50

[a]M is the magnitude of an earthquake on the Richter scale.
[b]Width at base of 4800 m.

Table 2. Major rock types and thicknesses of the formations in the Tsao-Ling area

Epoch	Formation	Major rock types	Thickness (m)
Holocene	Alluvium	Silt, sand, and gravel	1–50
Holocene	Colluvium	Silt, sand, and rock blocks	1–170
Pleistocene	Terrace deposits	Sand and gravel	1–10
Pliocene	Cholan Formation	Thick clayey sandstone interbedded with shale or silty sandstone	>1000
Pliocene	Chinshui Shale	Thick, dark gray mudstone and interbedded shale and sandstone	80–150
Miocene	Dawuo Sandstone	Thick clayey sandstone interbedded with shale	~100
Miocene	Shihliufen Shale	Thick shale with occasional thin layer of sandstone	100

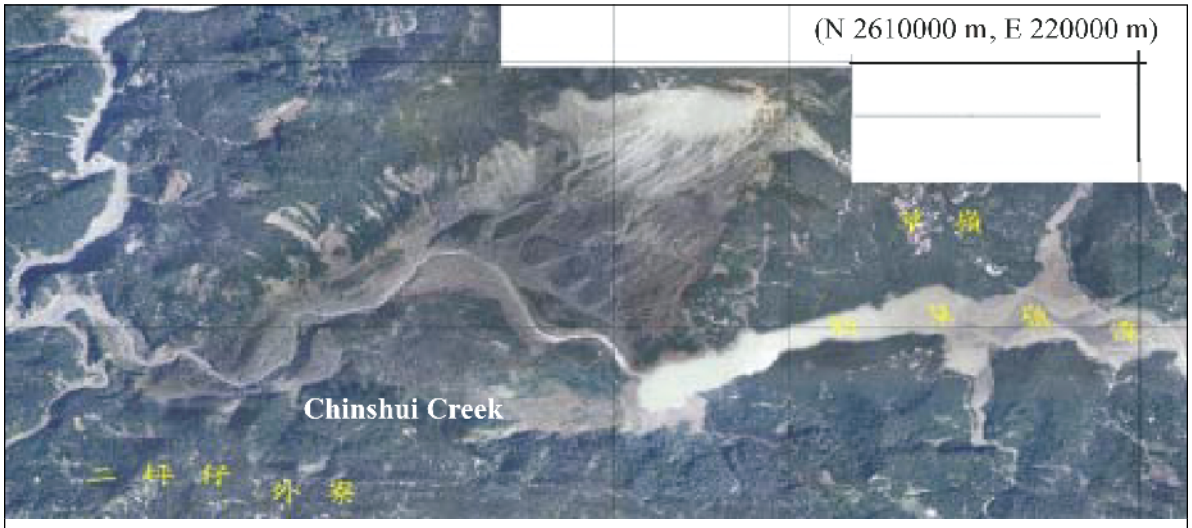

Figure 4. Aerial photograph mosaic of the Tsao-Ling landslide.

Thus, the shear strength of the soft rock layer decreases with time owing to seepage of water.

The major type of landslide in the Tsao-Ling area during the 921 earthquake was block sliding along the bedding planes between sandstone and shale, both in the Cholan Formation and in the Chinshui Shale, at the southwestern side of the mountain. The other types of collapse were falling rock because of the vertical joints in rock masses of cliffs and debris rolling and (or) sliding down slopes into the valley bottoms.

Applications of remotely sensed data

The exact causes of landslides are difficult to determine and may be the result of one or a combination of several natural causes. Thus, civil engineers need to place a great effort on investigation and analysis to gain proper information and control the unstable slopes to prevent the damage from other landslides.

Besides knowledge of the geological conditions, a long-term monitoring program of the Tsao-Ling landslide is considered the most essential task for rehabilitation of the damaged area after the 921 earthquake. In addition to the temporal and spatial concerns of data, financial constraints and physical limitations hamper a complete field survey of such a large area with a need for frequent monitoring. Remote sensing was used in response to these deficiencies in acquiring terrain data.

Remote sensing provides a method for acquiring regular and recent information about terrain variations. The advantages of this method include (*i*) comprehensive coverage of an area, (*ii*) relatively low cost, (*iii*) ease of obtaining topographic details, and (*iv*) compatibility between digital remotely sensed data and numerical analysis programs. Remote sensing has been recognized as a useful tool to process spatial data and display results. It can be used to handle a variety of datasets, provide an effective assessment of remedial measures, and aid in a decision analysis. Gupta and Joshi (1990) and Lin et al. (2000; 2002) used remote sensing and geographic information system (GIS) techniques to assess the probable occurrence of landslides and debris flows. Another significant advantage of remote sensing and GIS techniques over the traditional numerical methods is their capability of displaying the results of spatial assessments with ease and visualization. In this research, remote sensing imagery was processed through ERDAS IMAGINE® (Leica Geosystems, Heerbrugg, Switzerland), an image processing and GIS package, to identify the terrain characteristics of the landslide.

Data analysis and results

To efficiently locate areas with high probability of landslide occurrence, a set of affecting factors was selected according to the analysis of the historical events and failure mechanisms. As mentioned previously, there are several factors affecting the stability of Tsao-Ling slopes, such as rainfall, earthquakes, rock formation, geological structure, and terrain characteristics. Rainfall and earthquakes are external forces acting as the triggering mechanism of the landslides and will have the same impact on the entire Tsao-Ling region. Landslides did not occur everywhere, however, because of the differences in geological conditions and (or) terrain characteristics (aspect, slope, and vegetation conditions, mainly). The geological formations and attitudes seldom change spatially and temporally, in contrast with the terrain characteristics that vary comparatively frequently because of natural and human forces. Thus, an efficient, long-term, yearly–quarterly monitoring program should focus on monitoring the variation of the terrain characteristics in the Tsao-Ling area.

Georegistered remote sensing data make it easier to interpret the terrain factors to evaluate the probability of occurrence of a landslide. Both photogrammetric data and satellite images were used to produce thematic maps of terrain factors affecting landslide occurrence, including slope, aspect, and vegetation condition. Also, the impact from the most important geological factor, namely dip direction, was included in the consideration

of aspect. The data analysis procedures are explained in the following sections.

Photogrammetric data

Topographic maps were created to determine the configuration of the landslide by photogrammetric method (stereoscopic aerial photographs). Hundreds of partially overlapping vertical aerial photographs were taken and processed to produce a grid of elevation pixels arranged systematically in rows and columns. A digital terrain model (DTM) was created to show the three-dimensional perspective of the landslide, including elevation, slope, and aspect. The byproduct is an animation of a virtual flight journey that helps in the visualization of the Tsao-Ling landslide.

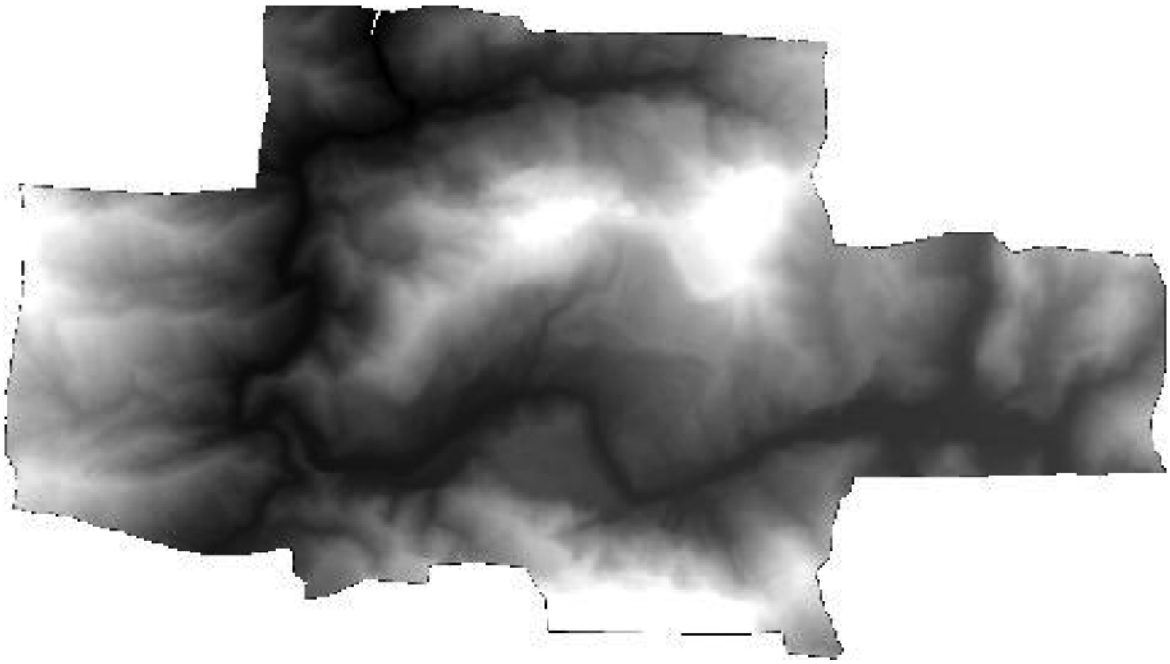

Figure 5. DEM of the Tsao-Ling landslide area before the 921 earthquake. Elevation varies in gray scale from 274.9 m (black) to 1297.6 m (white).

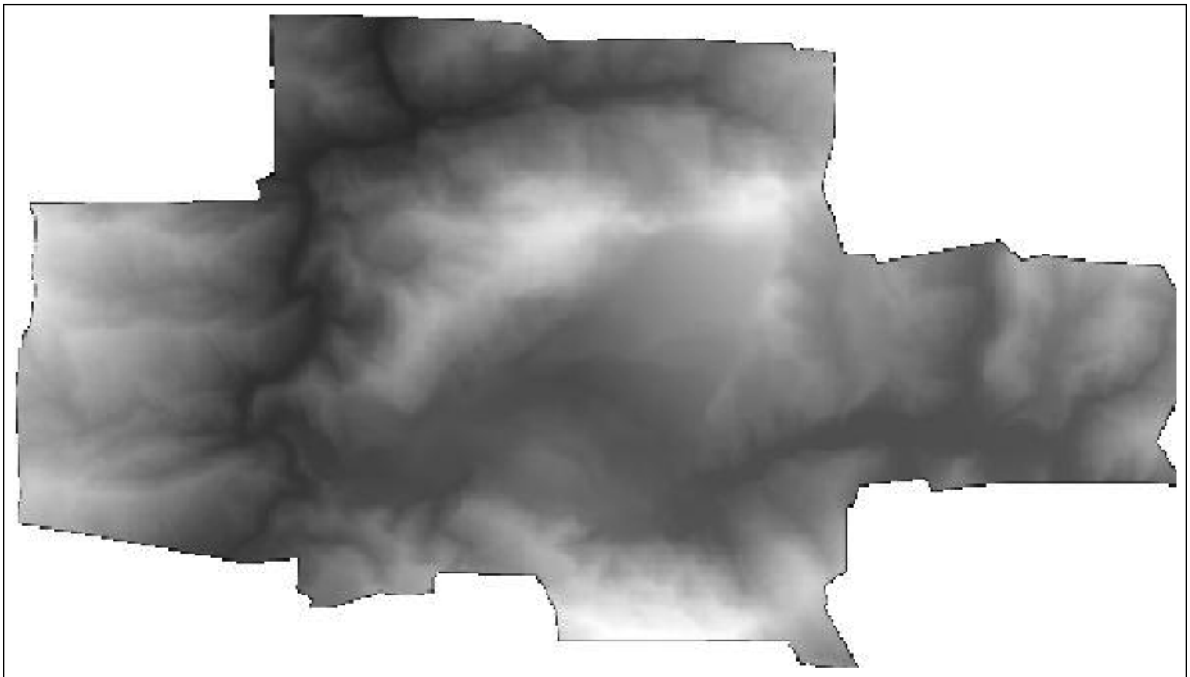

Figure 6. DEM of the Tsao-Ling landslide after the 921 earthquake. Elevation varies in gray scale from 275.0 m (black) to 1275.6 m (white).

Updated elevation data from the profile and cross section of the Tsao-Ling landslide area were generated based on stereo aerial photographs taken on 24 September 1999, three days after the 921 earthquake. Successive photographs were acquired under the designated flight lines, including an end lap of 75%, a side lap of 30%, an air base of 640 m, a flight height of 1200 m, and a nominal imagery scale of 1:8000. Kodak positive color film and a Zeiss RMK TOP 15/23 camera were used (Fourth River Basin Management Bureau, 1999). More than 200 photographs were taken to yield an aerial photograph mosaic of Chinshui Creek (see **Figure 4**). The elevation of the Tsao-Ling area was calculated with high spatial accuracy through geometric distortion correction. An elevation map was created with a contour interval of 0.5 m, and a digital elevation model (DEM) was generated at a ground resolution of 5 m × 5 m (each pixel size) with a resolution of 0.5 m in the *z* direction. Meanwhile, a set of historical stereoscopic photographs was used to create a DEM representing the topographic condition before the 921 earthquake for comparison (see **Figures 5 and 6**). Furthermore, two topographic layers, including aspect and slope digital data, were derived from the DEMs (see **Figures 7–10**). The aspect can be classified as north (N), northeast (NE), east (E), southeast (SE), south (S), southwest (SW), west (W), and northwest (NW) and was reassigned into class 1 (N, NE, and E), class 2 (SE and NW), class 3 (S), and class 4 (SW), since the dip direction of the Tsao-Ling region is in a southwest direction (see **Table 3**). Based on the possibility of a landslide caused by the slope angle, the slope has been categorized into four classes corresponding to 0–30°, 30°–50°, 50°–70°, and 70°–90° (see **Table 4**).

Soft-copy photogrammetry was applied in this research because of advantages such as timeliness and accuracy. The digital maps were created in a computer environment that is, therefore, available for GIS analysis. The digital maps can easily be represented as the product of mosaics and

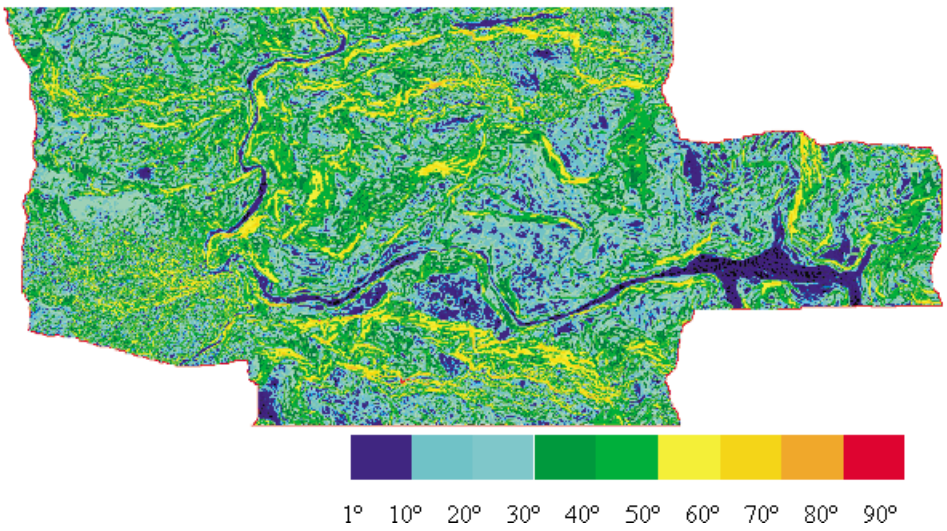

Figure 7. The slope distribution before the 921 earthquake.

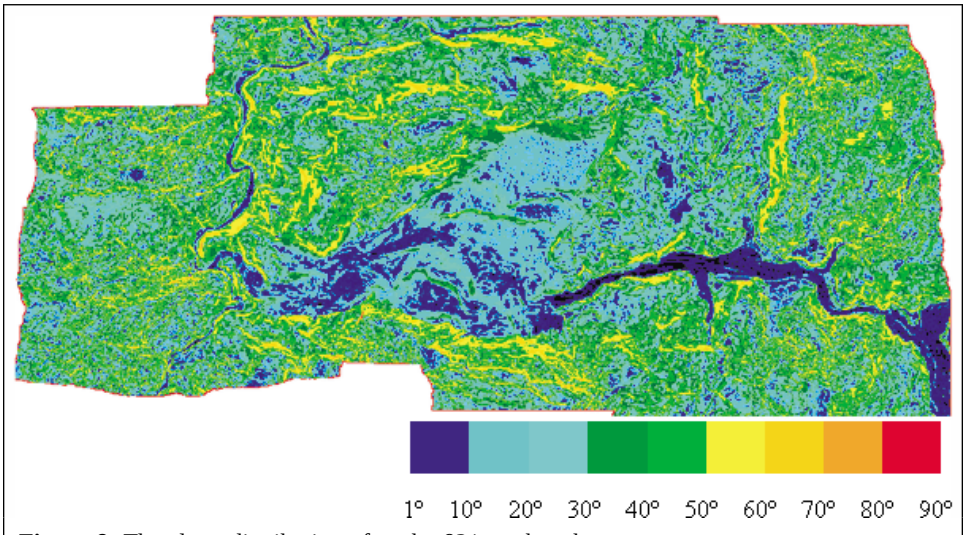

Figure 8. The slope distribution after the 921 earthquake.

orthophotographs and can also be used for a variety of image interpretation problems.

Satellite images

Another set of digital remotely sensed data were satellite images. A wide series of sensors on board Landsat, SPOT, and Indian Remote Sensing (IRS) satellites have proved to be an effective source of information to explore and monitor the earth's surface over the last decade (Jong and Burrough, 1995; Rao et al., 1996; Yang et al., 1996; 1999; Yang and Yang, 2004). The SPOT satellite can also derive a DEM because its high-resolution visible (HRV) imaging systems enable rotation of ±27° and gain stereoscopic images (Lillesand and Kiefer, 1994). Currently the elevation resolution of the satellite-derived DEM is less than that of photogrammetry-derived DEMs. DEMs were generated from stereo aerial photographs in this research but in other cases can be derived from SPOT images.

Multispectral SPOT imagery (with a path of K299 and a row of J303) was adopted in this research. Two SPOT XS images, shown in **Figures 2 and 3**, were taken before and after the earthquake, respectively. These two images are false-color imagery composed of a green band (0.50–0.59 μm), a red band (0.61–0.68 μm), and a near-infrared band (0.79–0.89 μm) with a ground spatial resolution of 20 m × 20 m (each pixel size).

The watershed of Chinshui Creek, about one million pixels in imagery (about 400 km^2 on the ground), was extracted from the original SPOT images. The objective for using the SPOT data was to rank soil conservancy according to vegetation condition. The normalized difference vegetation index (NDVI), which is a popular index analysis incorporating two bands of multispectral satellite imagery (Cihlar et al., 2003), was executed on the images to reveal the vegetation distribution over the Tsao-Ling area. NDVI values range between –1 and 1. High NDVI values indicate healthier and greater vegetation coverage. NDVI can be calculated as (Avery and Berlin, 1992) NDVI = (IR – R)/(IR + R), where IR is the infrared radiation

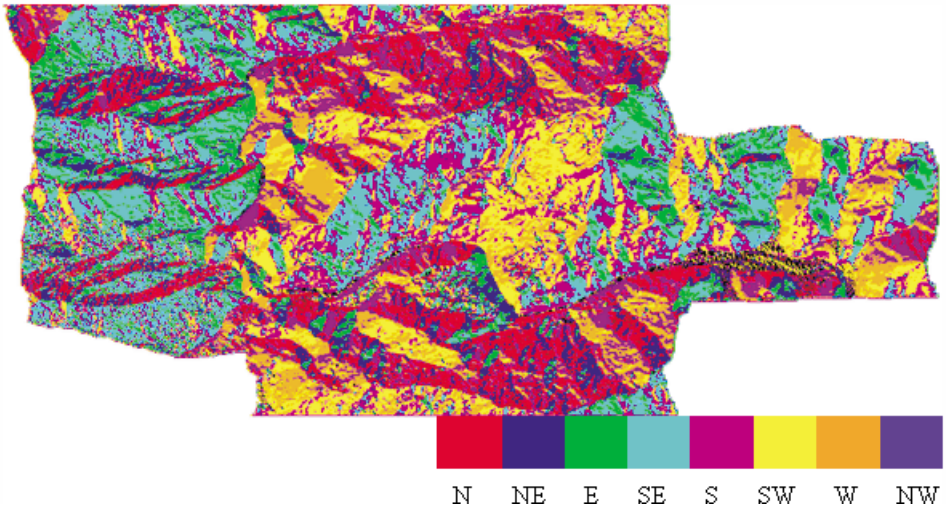

Figure 9. The aspect distribution before the 921 earthquake.

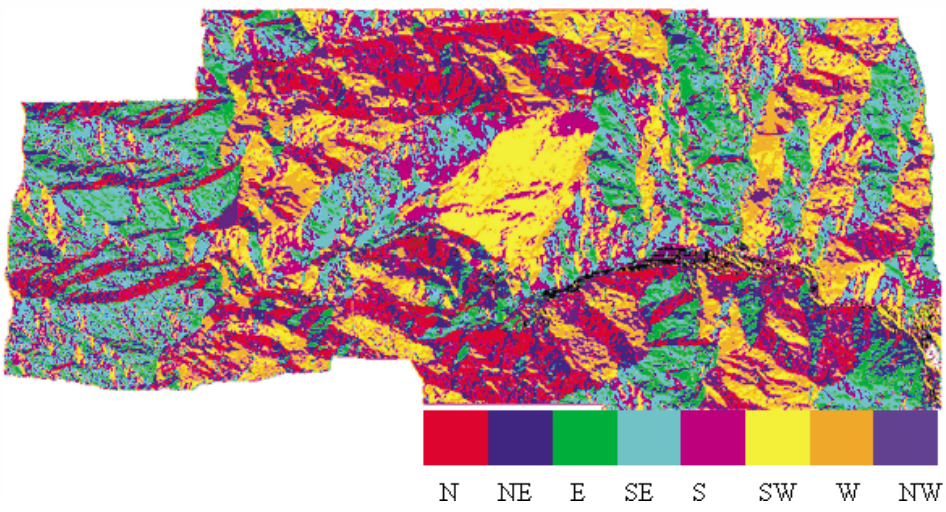

Figure 10. The aspect distribution after the 921 earthquake.

Table 3. Classification of aspect.

Direction to the north (°)	Aspect	Class
337.5–22.5	N	1
22.5–67.5	NE	1
67.5–112.5	E	1
112.5–157.5	SE	2
157.5–202.5	S	3
202.5–247.5	SW	4
247.5–292.5	W	3
292.5–337.5	NW	2

Table 4. Classification of slope.

Slope gradient (°)	Class
0–10	1
10–20	1
20–30	1
30–40	2
40–50	2
50–60	3
60–70	3
70–80	4
80–90	4

value and R is the red light radiation value. In SPOT imagery, band 2 represents red reflection, and band 3 near-infrared reflection. To compare the variation of the vegetation before and after the 921 earthquake, two images were analyzed with a time difference of 1 year in between. By processing these two SPOT images, the NDVI values were classified into four categories of vegetation conditions: healthy, fair, poor, and bare. The distribution of the vegetation conditions was overlaid onto the primitive gray-scale images (see **Figures 11 and 12**). Obviously, the vegetation condition worsened as a result of the 921 earthquake.

Thematic map of landslide probability

In addition to the geological investigation, this research considers three terrain factors (aspect, slope gradient, and vegetation condition) contributing to landslide occurrence that were derived from remotely sensed data. Based on the DEMs derived from aerial photographs, two derivative topographic layers, aspect and slope gradient, were generated. Vegetation condition is represented by NDVIs derived from SPOT images. In this analytical evaluation model, the quantitative affecting factors generated from mixed sources of data need to be standardized first. Four aspect classes were identified and weighted from 1 to 4 according to the direction relative to the dip direction of the Tsao-Ling region (about 230° to the north). The slope gradient was also classified into four classes and weighted from 1 to 4, depending on the affecting level of triggering a landslide: the greater the slope angle, the higher the

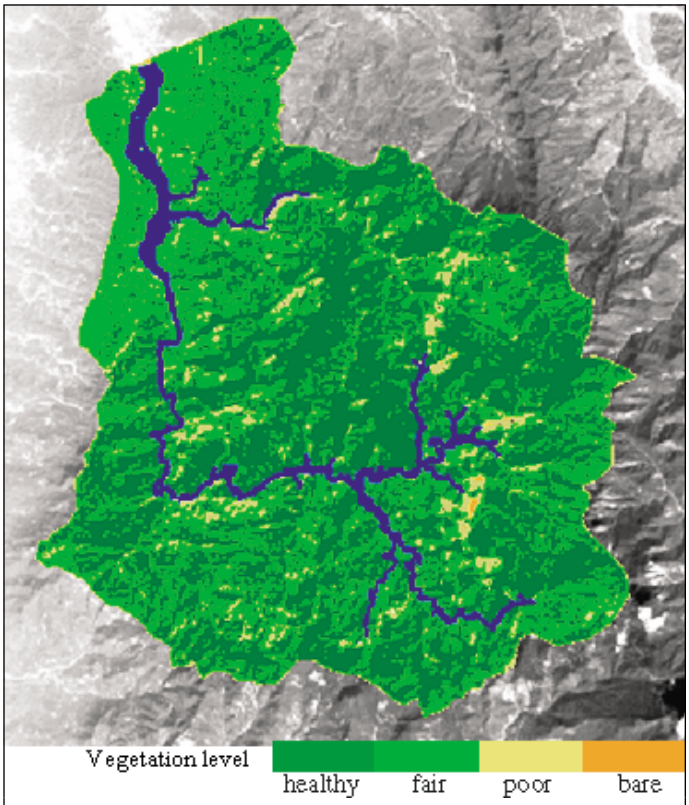

Figure 11. The vegetation condition of Chinshui Creek before the 921 earthquake.

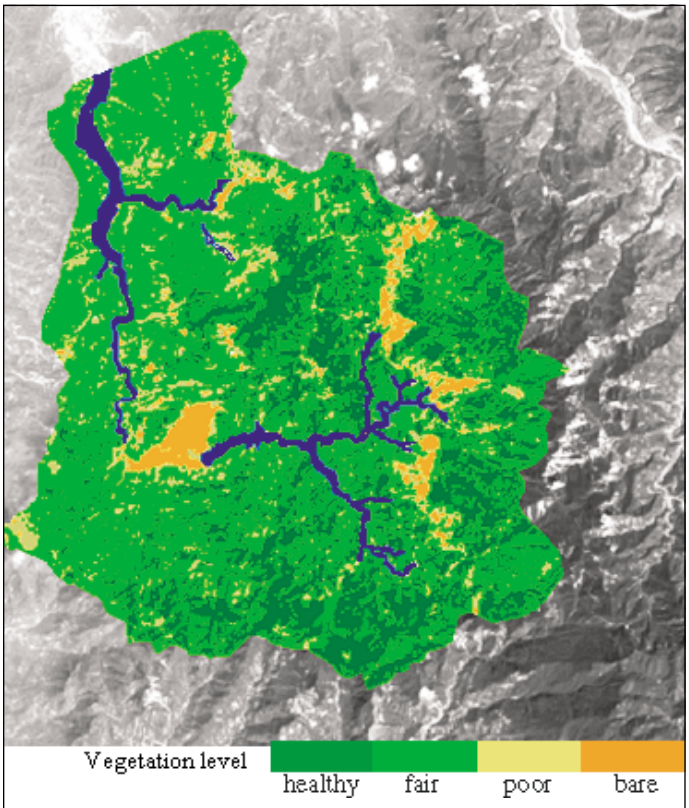

Figure 12. The vegetation condition of Chinshui Creek after the 921 earthquake.

possibility of a landslide. Similarly, the digital values of NDVI were classified and weighted into four ranks of vegetation condition: healthy (1), fair (2), poor (3), and bare (4). The image process of a superimposition of aspect, slope, and vegetation condition resulted in a probability distribution of landslide occurrence, as shown in **Figure 13**.

The overall affecting scores combining three terrain factors were processed by a linear aggregation function to produce the final evaluation. The affecting importance is represented by an equal weight, so three affecting scores were summed to give the final scores: the higher the affecting score, the higher the affecting level (i.e., higher possibility for a landslide to occur). The overall affecting scores were then classified into four probability classes (high, fair, low, and little) on a probability map of landslide occurrence.

Figures 14 and 15 are the probability maps resulting from the combined consideration of vegetation condition, slope, and aspect for the Tsao-Ling area before and after the 921 earthquake. This thematic map was also overlaid onto the primitive gray-scale images to show the results in association with geographic characteristics. **Figure 14** shows the landslide occurrence probability over the Tsao-Ling area before the 921 earthquake. Almost all landslides triggered by the 921 earthquake are located in the high-probability area of landslide occurrence in **Figure 14**. This result proves that the probability map of landslide occurrence is capable of providing valuable information for landslide evaluation. **Figure 15** represents the probability of landslide reoccurrence in the Tsao-Ling area and can be a reference for decision-makers to create treatment and rehabilitation plans.

Conclusions

To efficiently locate areas with high probability of landslide occurrence, a set of affecting factors was selected according to the analysis of historical events and failure mechanisms. The slope, aspect, and vegetation maps were generated from aerial and satellite images and were then overlaid to generate a map of potential landslide occurrence. During the first stage of damage assessment in the Tsao-Ling region after the 921 earthquake, remote sensing overcomes the temporal and spatial difficulties of in situ investigation as an ancillary monitoring tool. Both airborne and satellite images were used in this research to compensate for the deficit of in situ data for the classification of potential risk of landslide reoccurrence in the Tsao-Ling area. One can determine the locations of unstable slope to isolate areas that need detailed in situ geologic investigation. The probability maps of landslide occurrence were prepared based on aspect (related to geological condition), slope, and vegetation condition. Such thematic maps can provide useful information for an economic and rapid estimation of landslide stability for those areas where DEM, geological survey, and satellite imagery are available, such as all of Taiwan. Apparently, these remote sensing data provided economic and timely information for terrain monitoring that aided engineers

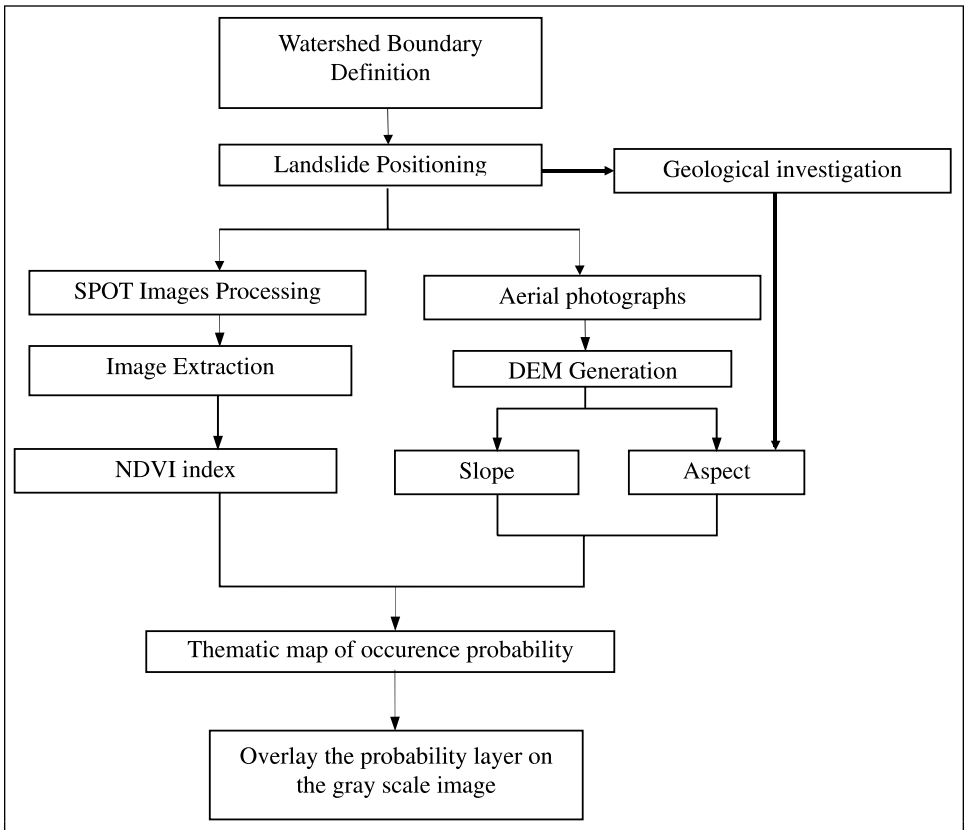

Figure 13. Flow chart showing the remotely sensed data process.

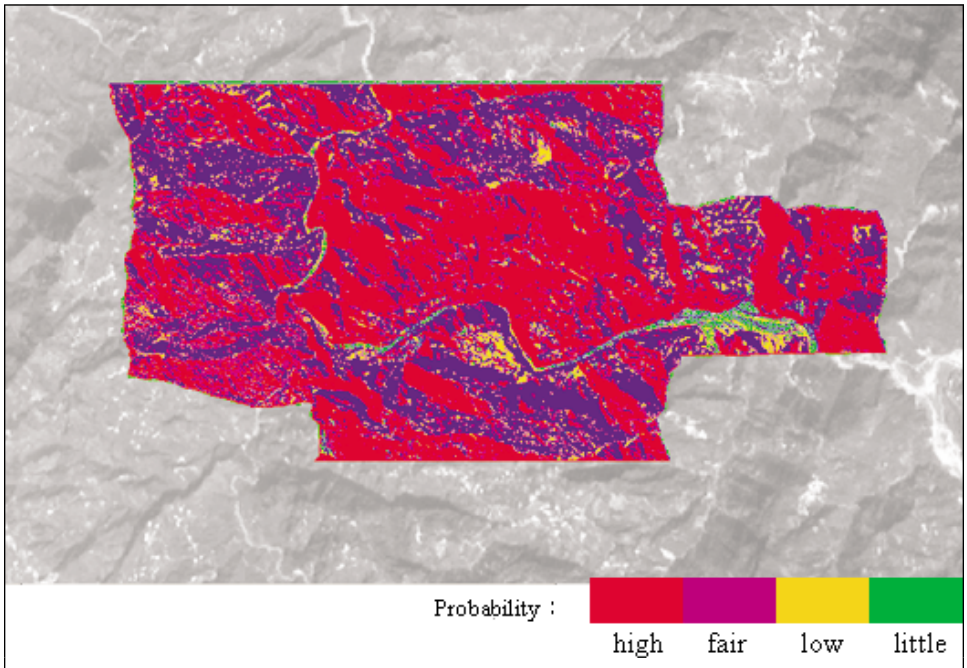

Figure 14. Superimposition of landslide probability distribution on an original gray-scale image before the 921 earthquake.

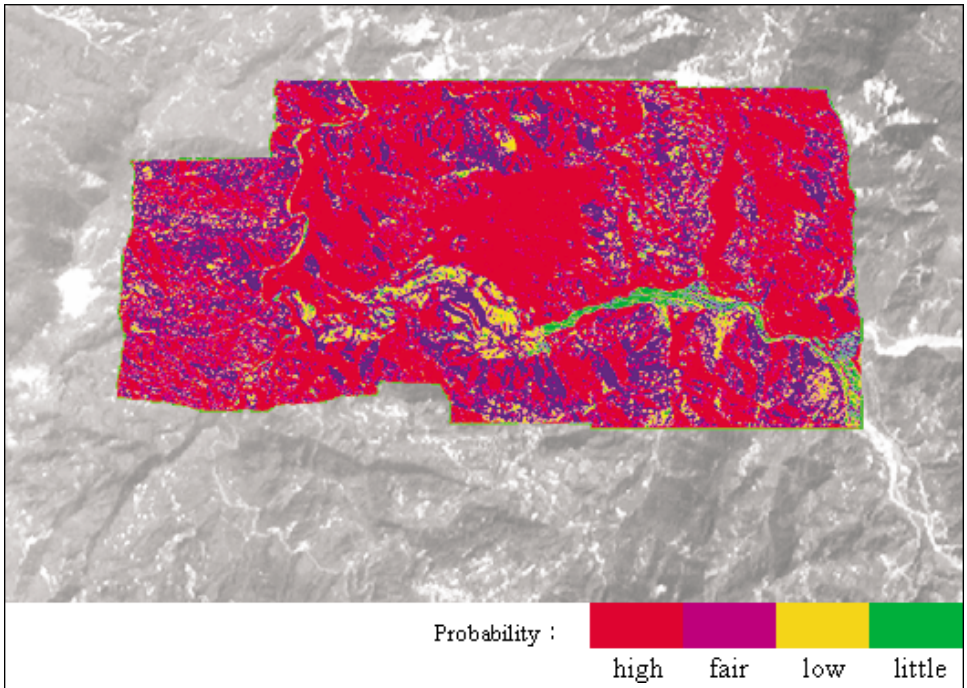

Figure 15. Superimposition of landslide probability distribution on an original gray-scale image after the 921 earthquake.

to easily understand the landslide susceptibility within a broad area over the long term.

It is evident that remote sensing provides superior spatial and temporal coverage for land surface monitoring and will become a major tool for landscape monitoring. Since the resolution of satellite images has become finer (e.g., QuickBird, IKONOS, and ROCSAT-2 imagery), remote sensing plays a more significant role in providing data to assess the impacts of natural and human forces on land resources.

References

Avery, T.E., and Berlin, G.L. 1992. *Fundamentals of remote sensing and airphoto interpretation*. 5th ed. MacMillan Publishing Company, New York. 472 pp.

Chang, S.C. 1984. Tsao-Ling landslide and its effects on a reservoir project. In *Proceedings of the 4th International Symposium on Landslides*, Toronto, Ont. Canadian Geotechnical Society, Downsview, Ont. Vol. 1, pp. 469–473.

Cihlar, J., Latifovic, R., Beaubien, J., Guindon, B., and Palmer, M. 2003. Thematic mapper (TM) based accuracy assessment of a land cover product for Canada derived from SPOT VEGETATION (VGT) data. *Canadian Journal of Remote Sensing*, Vol. 29, No. 2, pp. 154–170.

Fourth River Basin Management Bureau. 1999. *The aerial data generation plan of Tsao-Ling landslide dam*. Fourth River Basin Management Bureau, Water Conservancy Agency, Ministry of Economic Affairs. [In Chinese.]

Gupta, B.P., and Joshi, B.C. 1990. Landslide hazard zoning using the GIS approach — a case study from Ramganga Catchment, Himalayas. *Engineering Geology*, Vol. 28, pp. 119–131.

Hsu, T.L., and Leung, H.P. 1977. Mass movement in the Tsao-Ling area, Yu-Lin Hsian, Taiwan. *Proceedings of the Geological Society of China*, Vol. 20, pp. 114–118. [In Chinese.]

Hung, J.J. 1980. A study on Tsao-Ling rock-slides, Taiwan. *Journal of Engineering Environment*, Vol. 1, pp. 29–39. [In Chinese.]

Hung, J.J. 2000. Chi-Chi earthquake induced landslides in Taiwan. *Earthquake Engineering and Engineering Seismology*, Vol. 2, No. 2, pp. 25–33.

Institute of Planning and Hydraulic Research, Water Conservancy Agency, Ministry of Economic Affairs. 1996. *The planning report of treatment and management on Cho-Shui River.* Institute of Planning and Hydraulic Research, Water Conservancy Agency, Ministry of Economic Affairs. [In Chinese.]

Jong, S.M., and Burrough, P.A. 1995. A fractal approach to the classification of Mediterranean vegetation types in remotely sensed images. *Photogrammetric Engineering & Remote Sensing*, Vol. 61, No. 8, pp. 1014–1053.

Lillesand, T.M., and Kiefer, R.W. 1994. *Remote sensing and image interpretation*. John Wiley & Sons, New York. 721 pp.

Lin, P.S., Hung, J.C., Lin, J.Y., and Yang, M.D. 2000. Risk assessment of potential debris-flows using GIS. In *Debris-flow Hazards Mitigation: Mechanics, Prediction, and Assessment, Proceedings of the 2nd International Conference, 16–18 Aug. 2000, Taipei, Taiwan.* Edited by G.F. Wieczorek and N.D. Naeser. A.A. Balkema, Rotterdam, The Netherlands. pp. 431–440.

Lin, P.S., Lin, J.Y., Hung, J.C., and Yang, M.D. 2002. Assessing debris-flow hazard in a watershed in Taiwan. *Engineering Geology*, Vol. 66, pp. 295–313.

Rao, T.C.M., Rao, K.V., Kumar, A.R., Rao, D.P., and Deekshatula, B.L. 1996. Digital terrain model (DTM) from Indian Remote Sensing (IRS) satellite data from the overlap area of two adjacent paths using digital photogrammetric techniques. *Photogrammetric Engineering & Remote Sensing*, Vol. 62, No. 6, pp. 727–731.

Water Conservancy Agency. 1999. *The final report of treatment on 921 earthquake area — Tsao-Ling area*. Water Conservancy Agency, Ministry of Economic Affairs. [In Chinese.]

Yang, M.-D., and Yang, Y.-F. 2004. Genetic algorithm for unsupervised classification of remote sensing imagery. In *Image Processing: Algorithms and Systems III*. Edited by E.R. Dougherty, J.T. Astola, and K.O. Egiazarian. Proceedings of SPIE Vol. 5298. In press.

Yang, M.-D., Merry, C.J., and Sykes, R.M. 1996. Adaptive short-term water quality forecasts using remote sensing and GIS. In *Proceedings of the AWRA Symposium on GIS and Water Resources*, 22–26 Sept. 1996, Fort Lauderdale, Fla. Edited by C.A. Hallam, J.M. Salisbury, K.J. Lanfear, and W.A. Battaglin. American Water Resources Association, Herndon, Va. pp. 109–118.

Yang, M.-D., Merry, C.J., and Sykes, R.M. 1999. Integration of water quality modeling, remote sensing, and GIS. *Journal of the American Water Resources Association*, Vol. 35, No. 2, pp. 253–263.